Optical Characterization of Single-Walled Carbon Nanotubes Synthesized by Catalytic Decomposition of Alcohol

Shigeo Maruyama, Yuhei Miyauchi, Yoichi Murakami and Shohei Chiashi

Department of Mechanical Engineering, The University of Tokyo
7-3-1 Hongo, Bunkyo-ku, Tokyo 113-8656, Japan
TEL: +81-3-5841-6421, FAX: +81-3-5800-6983

Corresponding Author:
Shigeo Maruyama
E-Mail: maruyama@photon.t.u-tokyo.ac.jp

Abstract

The single-walled carbon nanotubes (SWNTs) synthesized by a catalytic decomposition of alcohol (Alcohol CVD method, ACCVD) are compared with HiPco SWNTs sample through optical spectroscopic measurements such as resonant Raman scattering, optical absorption and near infrared fluorescence. By ACCVD method, SWNTs were synthesized either on zeolite catalyst-support particles or directly on the surface of quartz substrate, where the latter case a simple dip-coat technique was employed for mounting the metal catalyst. In specific, morphological characteristics of as-grown SWNTs generated on zeolite support are presented using SEM and TEM revealing that the SWNTs produced by the proposed method possesses significant quality that is almost free from amorphous carbons or metal particle impurities. The quality and diameter distribution of SWNTs were investigated and discussed through the results of Raman scattering and optical absorption. The average diameter of SWNTs was slightly smaller for SWNTs grown on zeolite particles compared with HiPco SWNTs. Finally, fluorescent emission spectra from isolated SWNTs in aqueous surfactant suspension were measured for variable excitation wavelength to determine the structural (n, m) distribution of SWNTs. The narrower chirality distribution was demonstrated for ACCVD SWNTs grown on zeolite compared with HiPco SWNTs.

1. Introduction

The discovery of single-walled carbon nanotubes (SWNTs) [1] has invoked numerous research interests because of their unique physical properties [2] and hence remarkable potentials as a new material for vast possible applications. The production technique of SWNTs has been sought from the earliest period to respond to strong demands for the specimen with sufficient amount and quality. Following to the landmark establishment of the synthesis method in macroscopic amount [3, 4], several techniques employing CVD approach [5-18] has been proposed for the improved efficiency or productivity in the bulk synthesis of SWNTs. At present, CVD approaches including the high-pressure CO (HiPco) technique [8, 12] have become dominant for the mass production of SWNTs.

The present main issue concerning SWNTs production, therefore, is an enhancement of the quality that is critical for the reliable performance of proposed SWNT-based applications. The contamination (amorphous carbon or metal particle impurities) were often accompanied among the products as readily recognized from the pictures shown in the past literatures [8, 10, 12-16]. As one feasible solution to this concern, we have proposed the use of alcohol, especially ethanol and methanol, for the carbon feedstock [19, 20]. The proposed alcohol catalytic CVD (ACCVD) method can produce SWNTs with fine quality when combined with appropriate catalysts and experimental procedures. Furthermore, it was recently demonstrated that high quality SWNTs could be synthesized on the mesoporous-silica coated substrate [21] or directly on solid substrate such as silicon and quartz [22].

In this report, the quality of SWNTs synthesized from ethanol was investigated both qualitatively and quantitatively through several spectroscopic analyses. Throughout this report, the pristine HiPco sample supplied from Rice University (batch #: HPR113.4, using 1 ppm $Fe(CO)_5$, reaction pressure and temperature were 30 atm and about 950 °C, respectively) were employed as a reference for a comparison. First, the SEM and TEM studies were performed in order to discuss the quality as well as morphological characteristics of SWNTs grown on zeolite support powder. In the following, Raman scattering analyses and optical absorption measurement were fulfilled for the quantitative characterization of produced ACCVD SWNTs. Finally, chirality distribution of

produced SWNTs were determined by measuring fluorescence emitted from isolated SWNTs in aqueous suspension.

2. Experimental procedure and measurement

The detailed preparation of metal supporting zeolite powder was described in our past reports [19, 20]. We prepared a catalytic powder by impregnating iron acetate $(CH_3CO_2)_2Fe$ and cobalt acetate $(CH_3CO_2)_2Co\text{-}4H_2O$ onto USY-zeolite powder (HSZ-390HUA over 99 % SiO_2) [23, 24]. The weight concentration of Fe and Co was chosen to be 2.5 wt% each over the catalytic powder. Molybdenum acetate and cobalt acetate were employed for the catalytic loading onto the quartz substrate using dip-coat technique, whose detail procedure was presented in the previous report [22]. The adoption of Mo instead of Fe in the case of quartz is based on our knowledge obtained by preliminary experiments.

The schematic of our CVD apparatus and procedure of the CVD were presented in Refs. [25] and [20], respectively. In brief, the specimen was placed on a quartz boat and the boat was set in the center of a quartz tube (i.d. = 26 mm, length = 1 m). One end of the quartz tube was connected to a rotary pump by two different paths, one 25 mm and the other 6 mm diameter tubes to select the pumping efficiency. The central 30 cm of the quartz tube was surrounded with an electric furnace. While the furnace was heated up from room temperature, about 300 sccm of Ar/H_2 (3 % H_2) was flowed so that the inside of the quartz tube was maintained at 300 ± 20 Torr with only smaller evacuation path opened. After the electric furnace reached desired temperature, Ar/H_2 flow was stopped and the larger evacuation path was opened to bring the inside of the quartz tube vacuum. Subsequently, ethanol vapor was supplied from ethanol reservoir at a constant pressure of 10 Torr into the quartz tube. After the CVD reaction, the electric furnace was turned off and brought back to the room temperature with a 100 sccm flow of Ar/H_2. In this report, the CVD temperature of 850 and 800 °C are employed for the cases of zeolite powder and quartz substrate, respectively, because they are the optimum temperature when ethanol vapor pressure is 10 Torr [20, 22].

The synthesized SWNTs were characterized by FE-SEM (HITACHI, S-900) and TEM (JEOL 2000-EX). For the micro Raman scattering measurements, CHROMEX 501is and ANDOR

DV401-FI were used for the spectrometer and CCD system, respectively, with an optical system of SEKI TECHNOTRON STR250. In every Raman scattering measurement the spectrometer was calibrated using naphthalene and sulfur peaks. All Raman spectra presented in this report were an arithmetic average of the measurements at randomly chosen 5 different locations on the specimen. The VIS-NIR absorption spectra were measured with HITACHI U-4000. The fluorescence was measured with a spectrofluorometer of JOBIN YVON Fluorolog-311 with liquid nitrogen cooled InGaAs near IR detector.

3. SEM and TEM observations

Figure 1 shows SEM images of ACCVD SWNTs grown on zeolite (Fig. 1(a)) and HiPco SWNTs (Fig. 1(b)) taken in several magnifications. The CVD temperature and time of the sample in Fig. 1(a) is 850 °C and 60 min, respectively. The low magnification picture of Fig. 1(a) reveals that the zeolite particles of several hundreds of nanometers were integrated by web-like bundles of SWNTs. The surface of the zeolite powders was densely covered with SWNTs bundles with typical thickness of 10 - 20 nm. In the highest magnification, it was observed that the thinner bundles around/below 10 nm were seen preferably near the surface of the powder particle, and the bundle thickness seem to increase as they run around, due to van der Waals interactions, on the particle surface. At the outermost surface they finally seem to depart into space, where the bending stiffness of thereby thickened bundles could exceed the van der Waals forces from the surface. It is notable that our SWNT bundles are relatively straight and these walls are smooth, which is morphologically different from the bundles of HiPco SWNTs (Fig. 1(b)).

For more detailed investigation on structures, TEM images are compared in Fig. 2. The sample observed in Fig. 2(a) is same as that in Fig. 1(a). As expected from the above SEM observation, almost no amorphous carbon and metallic impurities were seen among the produced SWNTs even though this specimen was ‘as-grown’, as was confirmed by TGA [20]. The complete absence of metal particle impurities suggests that the catalytic metals were strongly adhered to the surface of zeolite during the CVD reaction. We ascribe the absence of amorphous carbon to an oxygen atom in ethanol molecule, which could selectively oxidize carbon atoms with dangling bonds

(i.e. candidate of amorphous carbon) into the form of more stable specie such as CO. On the other hand, the pristine HiPco SWNTs were accompanied with numerous iron particles around 2-5 nm in diameter in Fig. 2(b) as has been well described previously [12, 26].

4. Raman scattering analyses

The Raman analysis is a strong tool for the characterization of SWNTs [27], from which the quality and diameter distribution are estimated and metal-semiconducting distinctions are possible to some extent. The interpretation of Raman spectra of SWNTs should be referred to e.g. Ref. [28]. Figure 3 shows Raman spectra of ACCVD SWNTs on quartz substrate, on zeolite particles, and HiPco SWNTs, measured with an excitation of 488 nm laser. The CVD conditions of the zeolite and quartz samples were 850 °C × 10 min and 800 °C × 60 min for the CVD temperature and time, respectively. These temperatures are the optimum for both zeolite and quartz cases when Ar/H_2 is flowed during the heat up of the electric furnace. In any cases, the height of D-band around 1350 cm^{-1} is sufficiently smaller than G-band around 1590 cm^{-1}, indicating that the defects in the tube wall is sufficiently small. Note that, however, G/D ratio is just a quick estimation of SWNT quality and does not always reflect the quality sensitively as shown in Figs. 1 and 2.

Figure 4 shows the radial breathing modes (RBMs) of these SWNTs measured with three different excitation laser wavelengths of 488, 514.5, and 633 nm. Because of the resonance feature of Raman scattering of SWNTs due to the van Hove singularity of electronic DOS, RBM signals with 3 excitation energies are compared with the Kataura plot [29] calculated with $\gamma_0 = 2.9$ eV and $a_{c\text{-}c} = 0.144$ nm [30, 31] on top of Fig. 4. Here, the diameter d (nm) of SWNTs was estimated from the RBM Raman shift ν (cm^{-1}) using the relationship $d = 248 / \nu$ [30, 31]. The change in the resonant condition with 514.5 and 488 nm excitation can be understood from the Kataura plot. However, the resonant condition in this plot is apparently violated in the 633 nm measurements of all 3 case as denoted by asterisks in Fig. 4(g, h, i). A probable reason is the resonance condition of the i*th* valence van Hove singularity level to the i±1*th* level because the resonance occurs with the light polarized perpendicular to the nanotube axis [32, 33]. Nevertheless, the rough measure of diameter distribution can be obtained by these RBM measurements. While HiPco SWNTs and ACCVD

SWNTs on zeolite have remarkable similar diameter distribution of between 0.9 - 1.5 nm, ACCVD SWNTs grown on a quartz [22] substrate has thicker diameter between 1.1 - 1.8 nm.

5. Optical absorption

Optical absorption spectra of SWNTs were measured in several different techniques. Kataura et al. [29] dispersed SWNTs obtained by laser-oven method in ethanol and sprayed the suspension onto a quartz plate. O'Connell et al. [34] suspended HiPco SWNTs in D_2O solution with 1 % sodium dodecyl sulfate (SDS) in order to separate the bundled SWNTs into isolate ones. In addition, the absorption properties of 'as-grown' SWNTs can be measured by using a technique of synthesizing SWNT mat directly onto surface of quartz substrates [22], by which any effects of post-treatments are excluded. From the absorption peaks in the spectra, the electronic state of produced SWNTs is characterized since each peak corresponds to a band gap of obtained SWNTs.

Figure 5 compares optical absorption of (a) ACCVD SWNTs grown on quartz substrate, (b) ACCVD SWNTs grown on zeolite support, (c, d) HiPco SWNTs. All samples except Fig. 5(a) were prepared based on the procedure similar to O'Connell et al. [34]. The specimen in the pristine state was dispersed in 1 wt % SDS added D_2O by a sonication with a cup-horn sonicator (Hielscher GmbH, UP-400S) for 1 h at a power density of 460 W/cm^2. For the samples of Fig. 5(b) and (c), the suspension was further centrifuged under 20,627 g for 24 h and their supernatant rich with isolated SWNTs was used for the measurement.

Since the as-grown SWNTs on quartz in Fig. 5(a) are in the bundled state and not sonicated/dispersed in liquid at all, the peak separation is most ambiguous. The HiPco SWNTs sonicated and dispersed in D_2O (1 % SDS) but without centrifugation (Fig. 5(d)) shows slightly clearer peaks probably because some amount of isolated SWNTs exist along with bundled SWNTs. In comparing Fig. 5(a) and (d), it is recognized that the former has absorption peaks of slightly smaller energy. This coincides with the foregoing observation in Fig. 4 that SWNTs grown on quartz has larger diameter than that of HiPco SWNTs.

After the centrifugation and decanting of the sonicated HiPco and ACCVD samples, the absorption peaks become sharper, as demonstrated by O'Connell et al [34]. Slight blue shift was

observed from Fig. 5(c) to (d), which is due to the de-bundling of SWNTs [34]. Comparison of Fig. 5(b) and (c) implies that the ACCVD SWNTs grown on zeolite is thinner than HiPco SWNTs, judging from the absence of the peak around 1400 nm (i.e. thickest peak) in the case of Fig. 5(c). According to above sequential comparisons, the diameter order is estimated to be (ACCVD on zeolite) < (HiPco) < (ACCVD on quartz), that coincides with the results in Fig. 4.

From a comparison with the Kataura plot, the absorption peaks around 1000 - 1500 nm correspond to the first band of semiconducting SWNTs and peaks around 700 - 900 nm is considered to correspond to the second band gap of them.

6. Fluorescence measurement and structural determination

In order for the further characterization of produced SWNTs, we performed a spectrofluorimetric measurement, which is a strong tool for the quick determination of SWNT chiral distribution (n, m) recently proposed by Bachilo et al. [35]. The procedure in the sample preparation is the same as that used in Fig. 5. SWNTs were first dispersed in 1 wt % SDS-added D_2O solution using a cup-horn sonicator for 1 h, and then the suspension was centrifuged under 20,627 g for 24 h. Here, ACCVD SWNTs with zeolite support was directly used for the initial sonication. The supernatant including isolated SWNTs was used for the measurement.

Figures 6(a) and (b) shows the contour plots of fluorescence intensities for ACCVD and HiPco SWNTs, respectively, represented by the wavelengths of excitation (ordinate) and resultant emission (abscissa). The fluorescence emitted in a range of 900 to 1300 nm was recorded while excitation wavelength was scanned from 500 to 900 nm. The ACCVD SWNTs used in Fig. 6 (and following Fig. 7) were produced on zeolite support powder under the conditions of '850 °C, 10 min' for the CVD temperature and reaction time, respectively. Each distinct peak observed in Fig. 6 corresponds to fluorescence from a first band gap E_{11} of a semiconducting SWNT excited in a second band gap E_{22} with specific chiral (n, m). The positions of peaks were almost exactly the same as measurements by Bachilo et al. [35]. Even though the employed Kataura plot [36] and diameter-RBM frequency relations were inconsistent with those used for our Raman scattering analysis in Fig. 4, the chirality assignment by Bachilo et al. was temporarily adopted in Fig. 6.

Apparently, 2 major peaks of chiral indexes (7, 5) and (7, 6) were prominent for ACCVD SWNTs, while several more peaks were as strong as these peaks for HiPco SWNTs.

Figure 7 shows the distribution of diameter and chiral angle of synthesized SWNTs for both ACCVD and HiPco, where the area of a circle at each chiral point denotes the strength of the fluorescence measured in Fig. 6. Since no information of chirality dependent quantum yield of absorption and emission is known, it is assumed that the strength of fluorescence closely resembled the abundance distribution. This figure shows a clear difference in the chiral distribution between these two samples. First, ACCVD SWNTs has narrower; at the same time smaller, diameter distribution while HiPco SWNTs has a relatively wider diameter distribution, which coincides with the result in Fig. 5. Second, the SWNTs grown from ethanol has a dominant distribution in higher chiral angle region close to so-called armchair type, while the HiPco SWNTs shows less remarkable dependence of the distribution on the chiral angle. Further investigations to elucidate the origin of this difference in chirality distribution are currently in progress by our group.

When this paper was in the final preparation stage, we found that Weisman et al. [37] has measured the chirality distribution of SWNTs generated from the CCVD method of Resasco, which used the CO-disproportional reaction on Co/Mo catalyst supported on silica (CoMo CAT) [10]. The resultant distribution has major peaks at (6, 5) and (7, 5). The whole distribution was remarkably similar to our ACCVD SWNTs generated at 750 °C as shown in Fig. 8 in the same fashion as in Figs. 6 and 7. It is suspected that the chirality distribution tends to be more armchair side when diameter of SWNTs is smaller.

7. Conclusion

We have characterized our SWNTs synthesized from ethanol by means of spectroscopic analyses using HiPco SWNTs as a reference specimen. Observations by SEM and TEM exhibited the fine quality of ACCVD SWNTs synthesized on zeolite support powder as well as the morphological difference between those two samples. The resonant Raman analyses with three different excitations 488, 514.5, and 633 nm were performed for ACCVD SWNTs grown on zeolite and quartz substrates, and HiPco SWNTs. It was shown that the ACCVD SWNTs grown on a quartz

surface has larger diameter distribution in the range of 1.1 - 1.8 nm, than ACCVD on zeolite and HiPco SWNTs. This was consistent with the optical absorption measurements where slightly thinner distribution of ACCVD on zeolite compared to HiPco SWNTs were confirmed. The detailed chiral distributions of latter two specimens were elucidated using spectrofluorimetric analyses. In addition that the tendency in diameter distributions coincides with the result observed in the optical absorption analyses, it was revealed that the ACCVD SWNTs had narrower chiral distribution where the tubes with higher chiral angle, i.e. close to armchair type, were dominant among them. This narrower chirality distribution observed in the case of ACCVD SWNTs could contribute to the future attempts to synthesize SWNTs with well restricted or even selected chirality.

Acknowledgements

The authors thank Mr. H. Tsunakawa (The University of Tokyo) for his assistance in TEM observations, Mr. T. Sugawara (The University of Tokyo) for his technical advices in FE-SEM observations, Prof. R. E. Smalley (Rice University) for supplying the HiPco sample, and Prof. R. B. Weisman (Rice University) for sending papers prior to publications. Part of this work was supported by KAKENHI #12450082 and 13555050 from JSPS, and #13GS0019 from MEXT.

References

[1] S. Iijima, T. Ichihashi, Nature 363 (1993) 603.

[2] R. Saito, G. Dresselhaus, M.S. Dresselhaus, Physical Properties of Carbon Nanotubes, Imperial College Press, London, 1998.

[3] A. Thess, R. Lee, P. Nikolaev, H. Dai, P. Petit, J. Robert, C. Xu, Y. H. Lee, S. G. Kim, A. G. Rinzler, D. T. Colbert, G. E. Scuseria, D. Tománek, J. E. Fischer, R. E. Smalley, Science 273 (1996) 483.

[4] C. Journet, W. K. Maser, P. Bernier, A. Loiseau, M. L. de la Chapelle, S. Lefrant, P. Deniard, R. Lee, J. E. Fisher, Nature 388 (1997) 756.

[5] H. Dai, A. G. Rinzler, P. Nikolaev, A. Thess, D. T. Colbert, R. E. Smalley, Chem. Phys. Lett.

260 (1996) 471.

[6] J. Kong, A. M. Cassell, H. Dai, Chem. Phys. Lett. 292 (1998) 567.

[7] J. H. Hafner, M. J. Bronikowski, B. R. Azamian, P. Nikolaev, A. G. Rinzler, D. T. Colbert, K. A. Smith, R. E. Smalley, Chem. Phys. Lett. 296 (1998) 195.

[8] P. Nikolaev, M. J. Bronikowski, R. K. Bradley, F. Rohmund, D. T. Colbert, K. A. Smith, R. E. Smalley, Chem. Phys. Lett. 313 (1999) 91.

[9] A. M. Cassell, J. A. Raymakers, J. Kong, H. Dai, J. Phys. Chem. B 103 (1999) 6484.

[10] B. Kitiyanan, W. E. Alvarez, J. H. Harwell, D. E. Resasco, Chem. Phys. Lett. 317 (2000) 497.

[11] M. Su, B. Zheng, J. Liu, Chem. Phys. Lett. 322 (2000) 321.

[12] M. J. Bronikowski, P. A. Willis, D. T. Colbert, K. A. Smith, R. E. Smalley, J. Vac. Sci. Technol. A 19 (2001) 1800.

[13] J.-F. Colomer, J.-M. Benoit, C. Stephan, S. Lefrant, G. Van Tendeloo, J. B. Nagy, Chem. Phys. Lett. 345 (2001) 11.

[14] W. E. Alvarez, B. Kitiyanan, A. Borgna, D. E. Resasco, Carbon 39 (2001) 547.

[15] B. Zheng, Y. Li, J. Liu, Appl. Phys. A 74 (2002) 345.

[16] W. E. Alvarez, F. Pompeo, J. E. Herrera, L. Balzano, D. E. Resasco, Chem. Mater. 14 (2002) 1853.

[17] L. Qingwen, Y. Hao, C. Yan, Z. Lin, L. Zhongfan, J. Mater. Chem. 12 (2002) 1179.

[18] A.R. Harutyunyan, B.K. Pradhan, U.J. Kim, G. Chen, P.C. Eklund, Nano Lett. 2 (2002) 525.

[19] S. Maruyama, R. Kojima, Y. Miyauchi, S. Chiashi, M. Kohno, Chem. Phys. Lett. 360 (2002) 229.

[20] Y. Murakami, Y. Miyauchi, S. Chiashi, S. Maruyama, Chem. Phys. Lett. 374 (2003) 53.

[21] Y. Murakami, S. Yamakita, T. Okubo, S. Maruyama, Chem. Phys. Lett. 375 (2003) 393.

[22] Y. Murakami, Y. Miyauchi, S. Chiashi, S. Maruyama, Chem. Phys. Lett. 377 (2003) 49.

[23] K. Mukhopadhyay, A. Koshio, N. Tanaka, H. Shinohara, Jpn. J. Appl. Phys. 37 (1998) L1257.

[24] K. Mukhopadhyay, A. Koshio, T. Sugai, N. Tanaka, H. Shinohara, Z. Konya, J. B. Nagy,

Chem. Phys. Lett. 303 (1999) 117.

[25] S. Maruyama, Y. Murakami, Y. Shibuta, Y. Miyauchi, S. Chiashi, J. Nanosci. Nanotech. in press.

[26] W. Zhou, Y. H. Ooi, R. Russo, P. Papanek, D. E. Luzzi, J. E. Fisher, M. J. Bronikowski, P. A. Willis, R. E. Smalley, Chem. Phys. Lett. 350 (2001) 6.

[27] A.M. Rao, E. Richter, S. Bandow, B. Chase, P.C. Eklund, K.A. Williams, S. Fang, K.R. Subbaswamy, M. Menon, A. Thess, R.E. Smalley, G. Dresselhaus, M.S. Dresselhaus, Science 275 (1997) 187.

[28] M. S. Dresselhaus, P. C. Eklund, Advances in Physics, 49 (2000) 705.

[29] H. Kataura, Y. Kumazawa, Y. Maniwa, I. Umezu, S. Suzuki, Y. Ohtsuka, Y. Achiba, Synth. Met. 103 (1999) 2555.

[30] R. Saito, G. Dresselhaus, M. S. Dresselhaus, Phys. Rev. B 61 (2000) 2981.

[31] A. Jorio, R. Saito, J. H. Hafner, C. M. Lieber, M. Hunter, T. McClure, G. Dresselhaus, M. S. Dresselhaus, Phys. Rev. Lett. 86 (2001) 1118.

[32] R. Saito, A. Grueneis, T. Kimura, A. Jorio, A.G.S. Filho, G. Dresselhaus, M.S. Dresselhaus, M.A. Pimenta, 58th Annual Meeting JPS 58 (2003) 825.

[33] A. Grüneis, R. Saito, Ge.G. Samsonidze, T. Kimura, M.A. Pimenta, A. Jorio, A.G.S. Filho, G. Dresselhaus, M.S. Dresselhaus, Phys. Rev. B 67 (2003) 165402.

[34] M.J. O'Connell, S.M. Bachilo, C.B. Haffman, V.C. Moore, M.S. Strano, E.H. Haroz, K.L. Rialon, P.J. Boul, W.H. Noon, C. Kittrell, J. Ma, R.H. Hauge, R.B. Weisman, R.E. Smalley, Science 297 (2002) 593.

[35] S.M. Bachilo, M.S. Strano, C. Kittrell, R.H. Hauge, R.E. Smalley, R.B. Weisman, Science 298 (2002) 2361.

[36] R.B. Weisman, S.M. Bachilo, Nanoletters, in press.

[37] S. M. Bachilo, L. Balzano, J. E. Herrera, F. Pompeo, D. E. Resasco, R. B. Weisman, J. Am. Chem. Soc., in press.

Captions to Figures

Fig. 1. SEM image in various magnifications of (a) ACCVD SWNTs on zeolite particles and (b) HiPco SWNTs. ACCVD SWNTs were synthesized under the condition of 850 °C and 60 min for CVD temperature and time, respectively.

Fig. 2. TEM images of (a) ACCVD SWNTs on zeolite particles and (b) HiPco SWNTs. Both samples are the same as in Fig. 1.

Fig. 3. Raman spectra of ACCVD SWNTs grown on quartz, ACCVD SWNTs grown on zeolite and HiPco SWNTs measured with 488 nm excitation. CVD conditions of ACCVD SWNTs on zeolite and that on quartz were 850 °C × 60 min and 800 °C × 60 min, respectively.

Fig. 4. Raman RBM spectra of samples compared in Fig. 3, measured with three different excitations of 488, 514.5, and 633 nm. On the top, the Kataura plot calculated with $\gamma_0 = 2.9$ eV and $a_{c\text{-}c} = 0.144$ nm is presented with the horizontal lines of corresponding laser energies.

Fig. 5. Optical absorption of (a) ACCVD 'as-grown' SWNTs directly synthesized on a quartz substrate, (b) ACCVD SWNTs, and (c, d) HiPco SWNTs. As for the samples (b-d), they were sonicated and dispersed in D_2O (1 % SDS). For 'isolated' samples (b, c), the suspension is centrifuged under 20, 627 g for 24 h and their supernatant were used for the exclusion of bundled SWNTs.

Fig. 6. Contour plots of fluorescence intensities for (a) ACCVD and (b) HiPco SWNTs, as a function of the wavelengths of excitation and resultant emission. ACCVD SWNTs were produced on zeolite support particles under the conditions of 850 °C and 10 min for the CVD temperature and reaction time, respectively.

Fig. 7. Diameter and chiral angle distribution of (a) ACCVD and (b) HiPco SWNTs where the area of the circle at each chiral point denotes the strength of the fluorescence.

Fig. 8. Fluorescence intensity and chirality distribution of ACCVD SWNTs produced on zeolite support under the conditions of 750 °C and 10 min for the CVD temperature and reaction time, respectively.

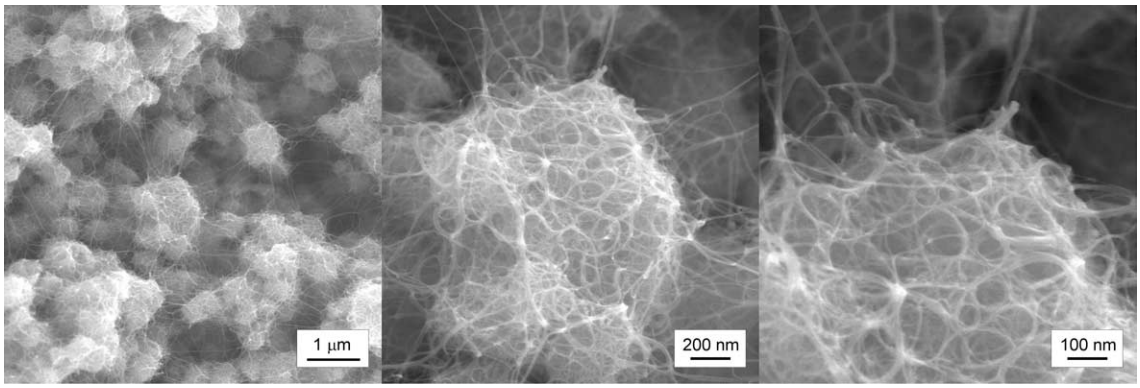

Fig. 1 (a)

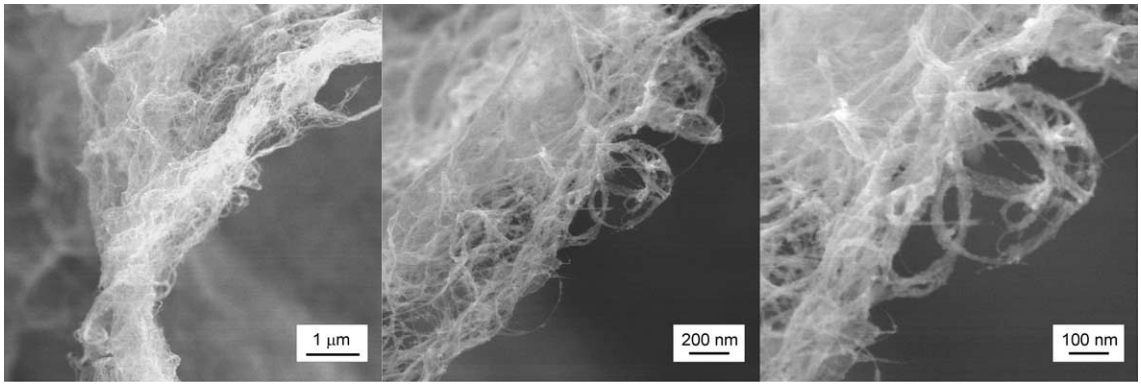

Fig. 1 (b)

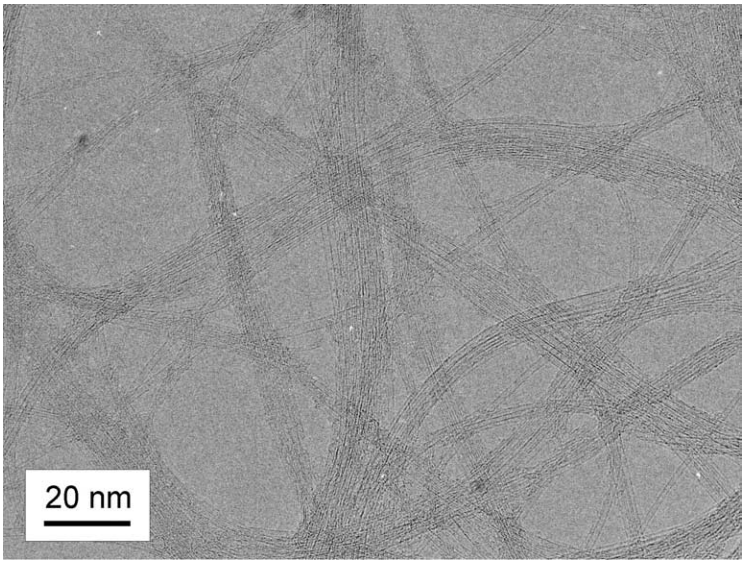

Fig. 2(a)

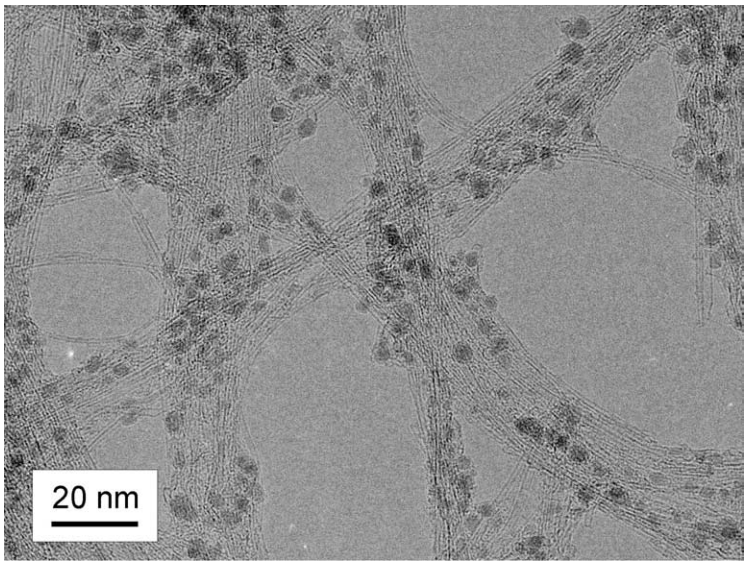

Fig. 2(b)

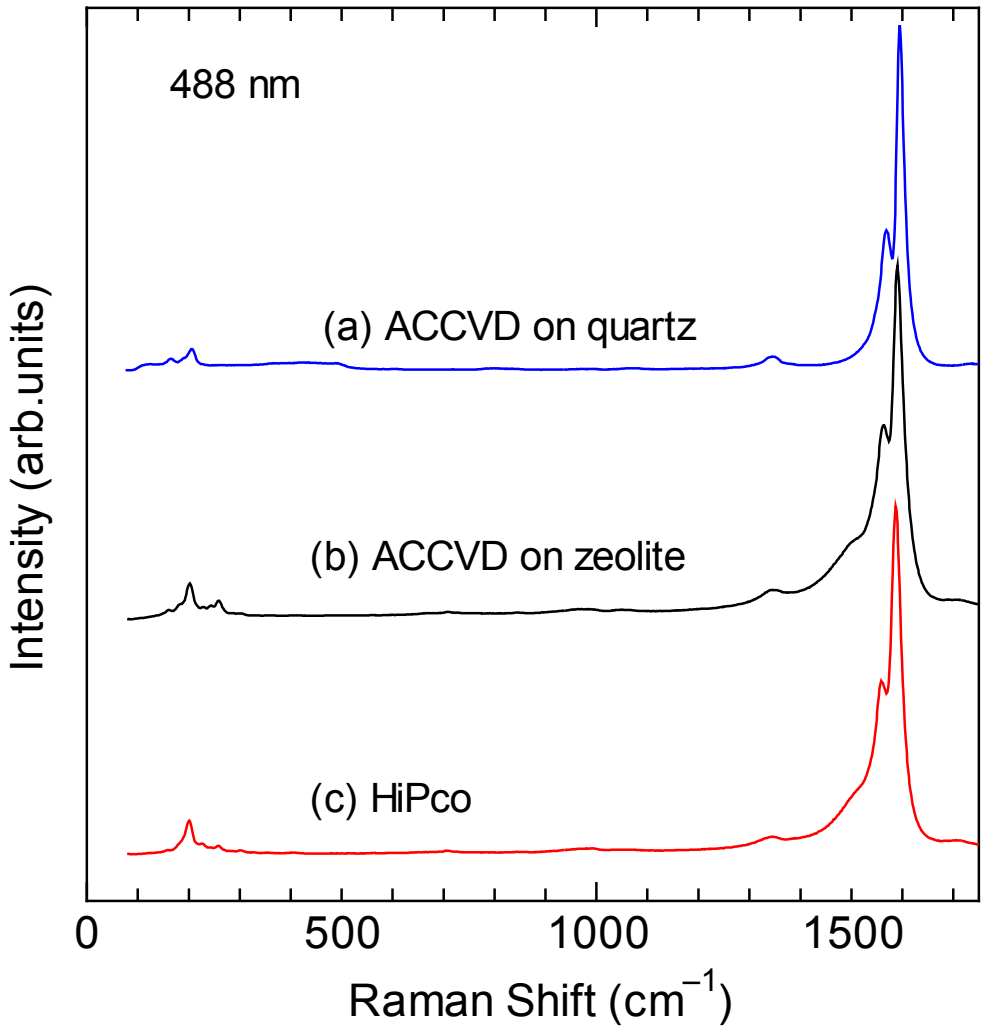
488 nm
(a) ACCVD on quartz
(b) ACCVD on zeolite
(c) HiPco
Intensity (arb.units)
0
500
1000
1500
Raman Shift (cm^{-1})

Fig. 3

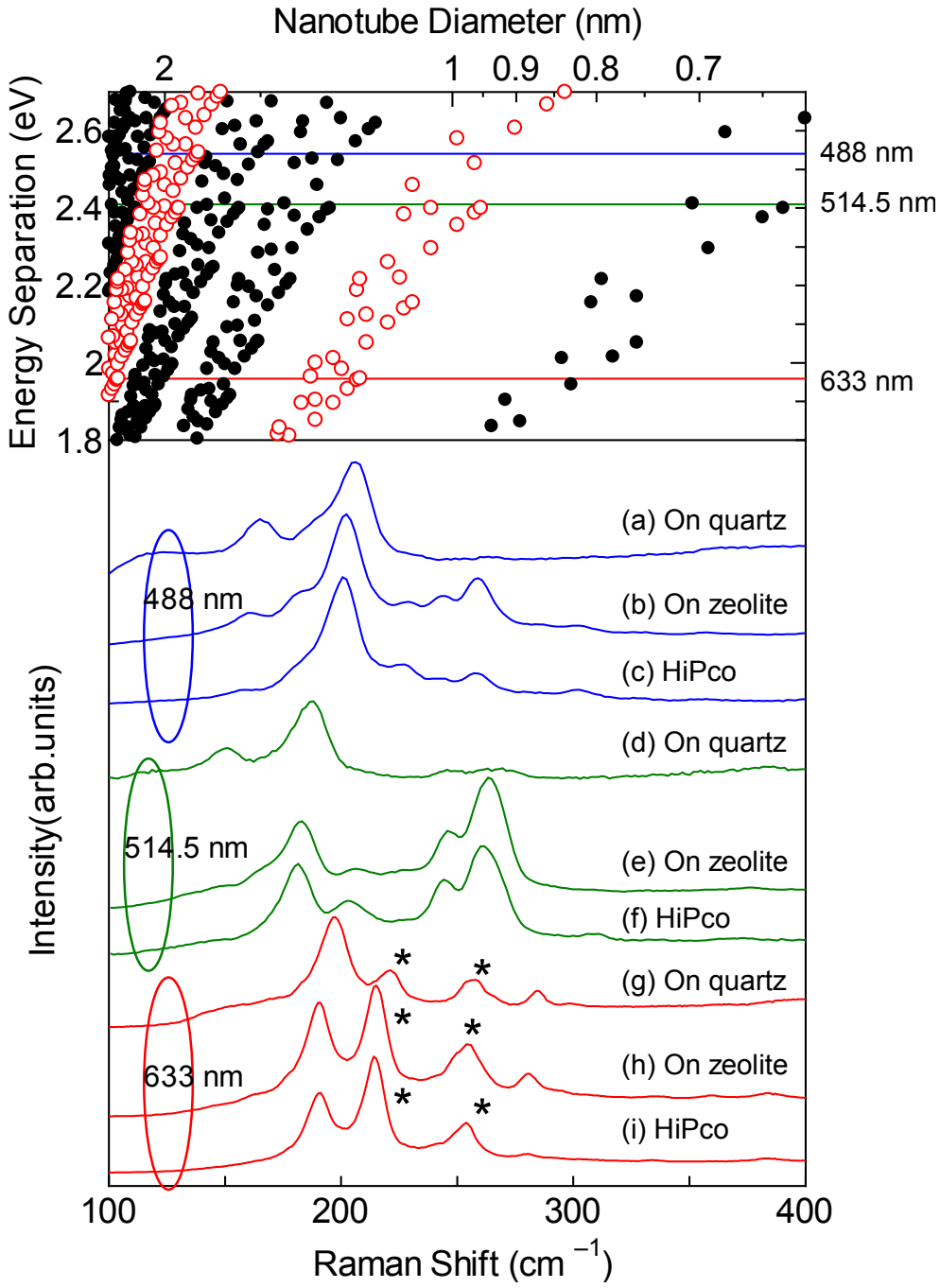
Nanotube Diameter (nm)
2
1
0.9
0.8
0.7
Energy Separation (eV)
2.6
2.4
2.2
2
1.8
488 nm
514.5 nm
633 nm
(a) On quartz
(b) On zeolite
(c) HiPco
(d) On quartz
(e) On zeolite
(f) HiPco
(g) On quartz
(h) On zeolite
(i) HiPco
488 nm
514.5 nm
633 nm
Intensity(arb.units)
100
200
300
400
Raman Shift (cm −1)

Fig. 4

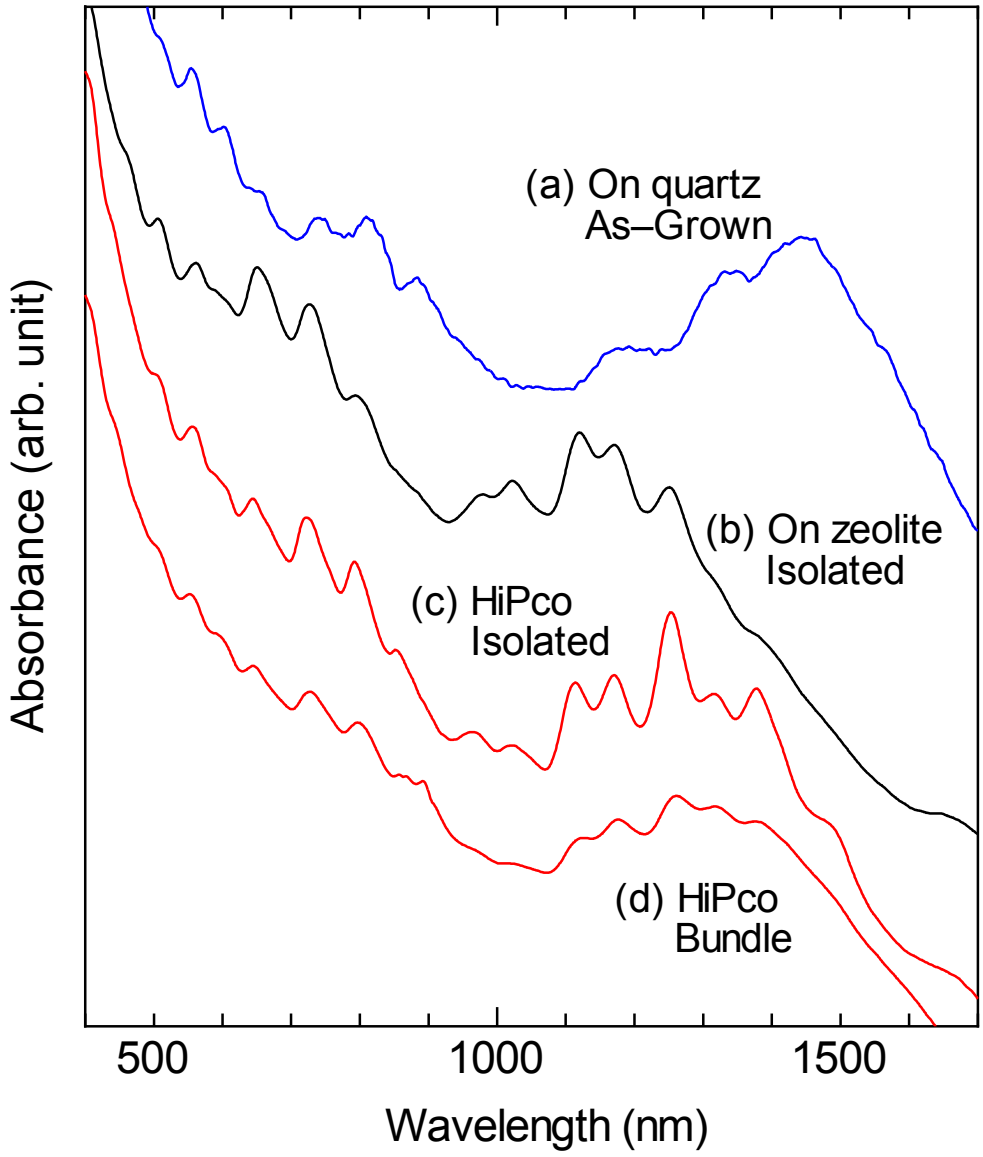
(a) On quartz
As–Grown
(b) On zeolite
Isolated
(c) HiPco
Isolated
(d) HiPco
Bundle
Absorbance (arb. unit)
500
1000
1500
Wavelength (nm)

Fig. 5

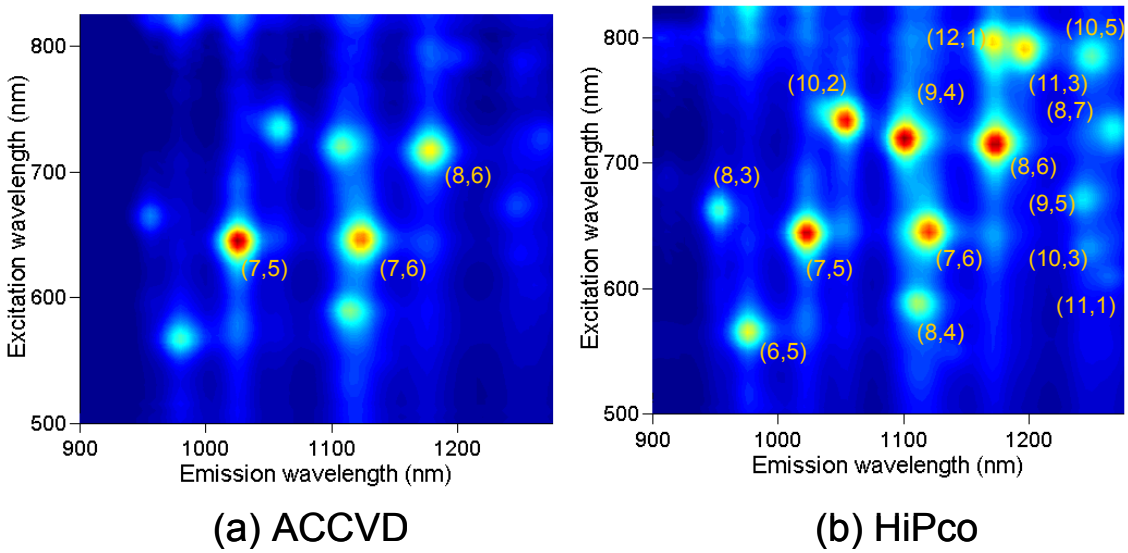
Excitation wavelength (nm)
800
700
600
500
900
1000
1100
1200
Emission wavelength (nm)
(8,6)
(7,5)
(7,6)
(a) ACCVD
(12,1)
(10,5)
(10,2)
(9,4)
(11,3)
(8,7)
(8,3)
(8,6)
(9,5)
(7,5)
(7,6)
(10,3)
(11,1)
(8,4)
(6,5)
(b) HiPco

Fig. 6

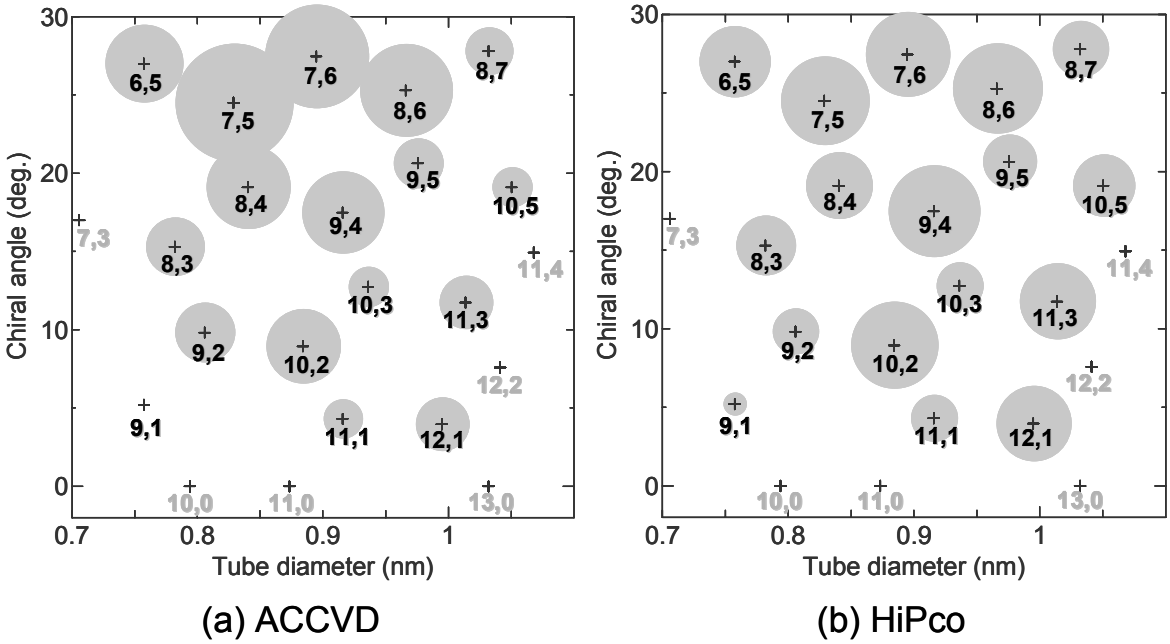
Chiral angle (deg.)
Tube diameter (nm)
6,5
7,6
8,7
7,5
8,6
9,5
8,4
9,4
10,5
7,3
8,3
11,4
10,3
11,3
9,2
10,2
12,2
9,1
11,1
12,1
10,0
11,0
13,0
(a) ACCVD
(b) HiPco

Fig. 7

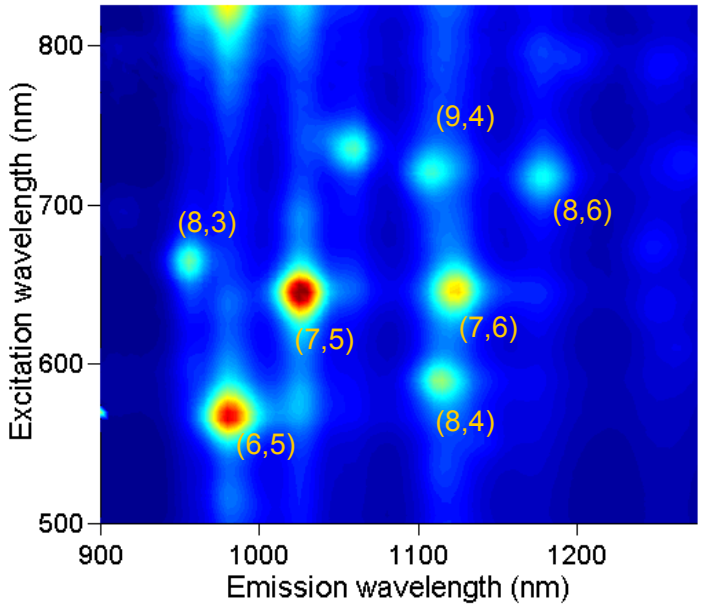
Excitation wavelength (nm)
800
700
600
500
900
1000
1100
1200
Emission wavelength (nm)
(9,4)
(8,3)
(8,6)
(7,5)
(7,6)
(8,4)
(6,5)

Fig. 8 (a)

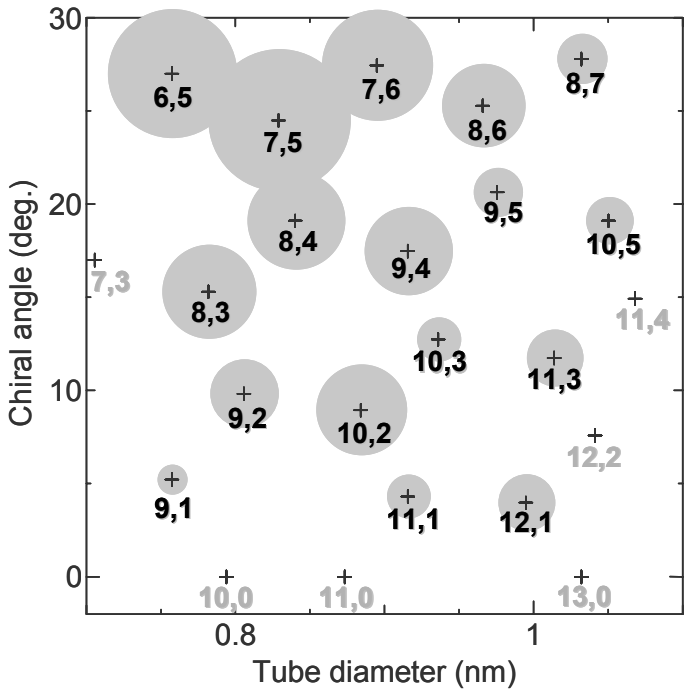
30
20
10
0
Chiral angle (deg.)
0.8
1
Tube diameter (nm)
6,5
7,5
7,6
8,6
8,7
9,5
10,5
8,4
9,4
7,3
8,3
11,4
10,3
11,3
9,2
10,2
12,2
9,1
11,1
12,1
10,0
11,0
13,0

Fig. 8 (b)